OPEN ACCESS Freely available online

Journal of Dental Sciences

Research Article

Effects of Naturally Collagen-derived Membranes from Bovine Pericardium and Dermis in Guided Bone Regeneration: An animal study in a cranial bone defect model

Yanqi Chen[1], Antian Xu[2], Siyuan Wang[2], Xiaoyu Chen[2], Yangbo Xu[2] and Fuming He[2*]

[1]*Department of Pediatrics, Stomatology Hospital, School of Stomatology, Zhejiang University School of Medicine, Clinical Research Center for Oral Disease of Zhejiang Province, Key Laboratory of Oral Biomedical Research of Zhejiang Province, Cancer Center of Zhejiang University, Hangzhou, China 310006.*

[2]*Department of Prosthodontics, Stomatology Hospital, School of Stomatology, Zhejiang University School of Medicine, Clinical Research Center for Oral Disease of Zhejiang Province, Key Laboratory of Oral Biomedical Research of Zhejiang Province, Cancer Center of Zhejiang University, Hangzhou, China 310006.*

ABSTRACT

Background/Purpose:
Naturally derived collagen membranes have garnered significant attention in GBR. However, scarce knowledge exists about the consequences of the usage of different tissue sources. The objective of this study was to explore tissue integration patterns of xenogeneic collage membranes from different animal species and tissues.

Material and Methods:
The materials derived from Bovine Pericardium (BP) and Dermis (BD) were characterized and compared to the Porcine-sourced Dermis membrane (PD). Histological, immunohistochemical and bone histomorphometrical methodologies were conducted at six time points in a cranial bone defect model using SD rats.

Results:
Characteristics analysis revealed that all membranes had a bilayer structure, with the BP membranes exhibiting a highest degree of purity in type I collagen. Histological results showed that both the BP and PD membranes initially displayed mild inflammation and vascularization within the bed implantation. The BP membranes demonstrated partial degradation with a stable rate over 16 weeks, whereas the PD membrane experienced nearly complete biodegradation. In term of bone regeneration and soft tissue healing, the BP membranes yielded outcomes comparable to those of the PD membranes. In contrast, the BD membranes provoked a strong foreign body reaction, which impeded tissue integration and osteogenic performance, despite exhibiting a high vessel density.

Conclusions:
An exuberant vascularization may not contribute to its tissue regeneration function. The BP membrane demonstrated optimal degradation behavior and superior barrier function, showing comparable results in both bone regeneration and soft tissue healing when compared to the PD membrane, which may serve as an ideal GBR membrane.

Keywords: collagen membrane; guided bone regeneration; degradation; tissue source, bovine-sourced pericardium

INTRODUCTION

Based on the application of a barrier membrane to cover an osseous defect, Guided Bone Regeneration (GBR) has become a widely used bone augmentation technique in oral and maxillofacial surgery [1, 2]. Naturally collagen-derived membranes, due to collagen being a principal component of connective tissue with excellent biocompatibility, have garnered significant interest [1, 3]. However, certain studies have reported that the collagen membranes have unfavorable mechanical properties, such as rapid degradation by collagenases, which compromises their barrier function [4, 5]. Therefore, it is of great importance to promote their degradation behavior while preserving barrier functionality and promoting tissue integration [6].

***Correspondence to** : Fuming He, Department of Prosthodontics, The Affiliated Stomatology Hospital, Zhejiang University School of Medicine, No.166, QiuTao Rd(N), Hangzhou 310020, China; Email: hfm@zju.edu.cn

Received: June 26, 2025**; Manuscript No:** JDSS-25-5373; **Editor Assigned:** June 30, 2025; **PreQc No**: JDSS-25-5373 (PQ); **Reviewed:** July 08, 2025; **Revised:** July 15, 2025; **Manuscript No**: JDSS-25-5373(R); **Published**: September 04, 2025

Citation: He F, Chen Y, Xu A, Wang S, Chen X, Yangbo X (2025), Effects of Naturally Collagen-derived Membranes from Bovine Pericardium and Dermis in Guided Bone Regeneration: an animal study in a cranial bone defect model. J Dent Sci, Vol.1 Iss.2, September (2025), pp:9-18.

Consolidation techniques, such as chemical cross-linking, have been used to enhance the stability of collagen membranes. However, these techniques have cytotoxicity and are associated with poorer tissue integration and delayed vascular invasion [6]. Previous studies have demonstrated that the choice of donor organisms (e.g., allogeneic or xenogeneic sources) and, more importantly, the tissue sources (e.g., dermis, pericardium, or tendon tissue) of collagen-based biomaterials significantly impact their physicochemical properties, integration behavior, and vascularization in a specific clinical context [7-9].

It is known that porcine dermis-derived collagen membranes are most often prematurely resorbed in 4-8 weeks, but it has been shown that they are "optimally" degraded via more or less physiological processes providing a good biocompatibility [10]. However, some scholars suggest that ideal GBR membranes should maintain its barrier function for 16-24 weeks to meet the requirement of different bone augmentation methods [11]. Researches have shown that collagen membranes derived from pericardium exhibited longer degradation time and enhanced barrier properties compared to those derived from dermis [8, 12]. Natural porcine-based pericardium membranes typically resorbed within 8 to 12 weeks in a dog model [12]. On the other hand, pericardium membranes from bovine had a resorption profile of 4 to 6 months [13]. However, bovine- based pericardium membranes exhibited delayed vascular penetration, which may impede bone regeneration [12, 14]. Nevertheless, some studies have reported positive effects of bovine pericardium bioavailability in enhancing bone reinforcement [15, 16]. Moreover, bovine-derived membranes have lower immunogenicity compared to porcine-derived collagen membrane, with only 3% of the population being allergic [17]. Thus, understanding the differences in tissue reaction to these materials can help in customizing composite materials for various applications in hard and soft tissue regeneration, based on clinical requirements such as fast vascularization and rapid degradation versus slow vascularization and tissue integration within the implantation bed [10].

However, for collagen-based membranes, only a few studies have analyzed the differences in various xenogeneic sources, and scarce knowledge exists about the consequences of the usage of different animal sources [18, 19]. Most of the membranes used in GBR procedures are based on porcine donor tissue. Fewer barrier membranes are used that originated from other animals or tissue origin [20]. To fill this knowledge gap, we applied three xenogenic collagen materials made from Bovine Pericardium (BP), from Bovine Dermis (BD) and from Porcine Dermis (PD) in this study. These membranes were implanted over a period of up to 16 weeks by means of an established cranial bone defect model in SD rats. The collagen-induced tissue reactions as well as their tissue integration patterns that involve cellular infiltration, vascularization, degradation and bone regeneration were investigated used by histological, immunohistochemical and bone histomorphometrical analysis in vivo.

MATERIALS AND METHODS

Material

This study utilized three representative commercial collagen membranes: 1) Bovine-sourced Pericardium membrane (BP, Megreen®, Shaanxi Reshine Biotech Co., Ltd, China); 2) Bovine-sourced Dermis membrane (BD, Heal-All®, Yantai Zhenghai Biotechnology Co., Shandong, China); and 3) Porcine-sourced Dermis membrane (PD, Bio-Gide®, Geistlich Pharma AG, Wolhusen, Switzerland). All three collagen membranes underwent similar preparation processes and were used as received, without any further modifications.

Materials characterization

The microstructure of the three membranes was observed under a Field-Emission Scanning Electron Microscope (FE-SEM, SU8010, Hitachi, Japan). Optical images were visualized by a stereo microscope (S9I, Leica, Germany) to show the surface morphology of the three membranes. The surface roughness, denoted as the arithmetic mean deviation of the profile (Ra), was calculated using a white-light interference microscope (NT9100, Veeco, America) (n = 3). Infrared spectra were collected using a Fourier Transform Infrared Spectroscopy (FTIR, Nicolet iS50, Thermo Fisher Scientific, USA) from 400 to 4000 cm^{-1}.

The water contact angle was measured at the moment a water droplet made contact with the sample using a contact angle goniometer (JC2000C, POWEREACH, China), and the average value was recorded. And the duration for a sample to absorb one droplet of water was recorded (n = 3).

The water absorption was determined by weighing the three materials before (W_{dry}) and after (W_{wet}) immersion in Milli-Q water for 5 seconds (n = 4). Water absorption rate = (W_{wet} _W_{dry})/W_{dry}. W_{wet} is the weight of the wet sample, while W_{dry} is the weight of the dry sample pre-weighed prior to immersion in Milli-Q water [21].

A hydroxyproline assay kit (A030-2-1, Nanjing Jiancheng Bioengineering Institute, China) was used to quantify the collagen content in the residual materials (n =3) after being incubated for 0, 5, 10, 15 and 20 min. Degradation ratio was calculated based on the OD values using the equation: Degradation Rate= $(A_{Sample}-A_{Blank})/(A_{Standard}-A_{Blank}) * C_{Standard} * V_{Hydrolysis}/W_{Sample}$.

Where:

A_{Sample} is the OD value of the sample's hydrolyzed supernatant.

A_{Blank} is the OD value of the blank's hydrolyzed supernatant.

$A_{Standard}$ is the OD value of the standard's hydrolyzed supernatant.

$C_{Standard}$ is the concentration of the standard (5 μg/ml).

$V_{Hydrolysis}$ is the total volume of the added hydrolysis solution.

W_{Sample} is the initial weight of the three membranes, which generally ranged between 13 and 15 mg.

Rat Cranial Defect Model

All experiments were conducted following the guidelines of the Institutional Animal Care and Use Committee (IACUC), ZJCLA, Hangzhou, China (Approval No. ZJCLA-IACUC-20030064). Male Sprague-Dawley (SD) rats (approximately 180-250 g) received intraperitoneal injections of sodium pentobarbital (50 mg/kg) and local lidocaine injections before surgery. After shaving and disinfection of the surgery area, the top of the rat skull was exposed and received a circular incision just before the sagittal suture on the left side. A cranial bone defect reaching the dura mater was then established using a circular drill with a diameter of 6 mm under continuous irrigation with physiologic saline solution. Subsequently, defects were stuffed with Gegreen calcined bovine bone (Shaanxi Reshine Biotech Co., Ltd, China) pre-immersed in physiologic saline solution and covered with the membranes of BP, BD, and PD, respectively [Fig. 2A]. The PD membrane was as the control group. Postoperatively, penicillin (100,000 U/d) was administered intramuscularly to prevent infection. Housing and husbandry conditions were approved by IACUC.

A total of 93 SD rats participated in the experiment and then randomly divided into three groups, with 5 rats per group at each time point (except for the 8-week time point, 6 rats per group). SD Rats were included in the study if they were healthy. At 16 weeks post-implantation, a total of 3 rats died naturally, comprising 2 from the PD group and 1 from the BP group. Rats were euthanized at designated time points for tissue analysis. Tissue healing on the smooth surface of the membranes was photographed using a digital camera. Cranial bones with substitute materials were then removed, dissected, fixed in 10% buffered formaldehyde and submitted to a 10% Ethylene Diamine Tetraacetic Acid (EDTA, Servicebio, China) for 3 weeks. The decalcified specimens were dehydrated in graded series of ethanol, then embedded in paraffin. Sections of 3-5 μm thick were cut for subsequent staining analysis.

Histological analysis

On week 1, 2, 4, 8, 12 and 16 after implantation, the specimens of each material were sectioned to prepare decalcified slices. Sections were used for histochemical staining, i.e., hematoxylin and eosin (H&E). All slices were analyzed by using a light microscope (BX53, Olympus, Japan).

The histological analysis was carried out according to the previous study [22]. The parameters included the infiltrating inflammatory cells (i.e., monocyte/macrophages, granulocytes, lymphocytes, Multinucleated Giant Cells (MNGCs)), fibroblasts, osteoblasts and connective tissue invasion on the different surfaces of membrane, so as to assess its histocompatibility and barrier function.

Moreover, the membrane's thickness was measured with ImageJ 1.53a software at the different time points. The membrane thickness was measured 3 times at different spots for each slide, using straight lines that were perpendicular to the membrane. And the number of samples in each group is 5-6.

Immunohistochemical analysis

In weeks 1, 2, and 4 after implantation, sections of each material were subjected to immunohistochemical staining for the CD31 marker, which is widely recognized as a specific indicator of endothelial cells. All slices were examined using a light microscope (BX53, Olympus, Japan). The vessel counting method was adapted from Said Alkildani [23], modifying the field of view from per mm^2 to 100x magnification. The intra-membrane vessel density (vessels per 100x) was quantified by counting the number of vessels in two randomly selected fields from each sample at 100x magnification, with five samples from each group analyzed using ImageJ software. Single endothelial cells or clusters of endothelial cells positive for CD31 was considered as individual vessels. The cells poorly resolved or stained were not counted.

DMicro-Computed tomography (Micro-CT analysis)

At the 8 and 12 weeks after surgery, the cranial bones were harvested and fixed by 4% paraformaldehyde (n = 6). The specimens were scanned using Micro-CT (U-CT- XUHR, Milabs, Netherlands) at high resolution. Images were reconstructed into a three-dimensional structure. New bone volume fraction (Bone Volume/Total Volume, BV/TV) was calculated in the total defect area (diameter of 6 mm, height of 2 mm) and the area adjacent to the membrane (diameter of 6 mm, height of 0.5 mm), respectively. Further, the proportion of bone formation adjacent to the membrane to the total bone formation in the defect area was evaluated.

Data analysis

Quantitative results were presented as mean ± standard deviation. In SPSS 25.0 software, the data were checked for normality (Shapiro-Wilk test) and homogeneity (Levene test). If both matched, statistical significance was determined by one-way analysis of variance (ANOVA) followed by LSD post-hoc multiple tests. If the data do not conform to the normality or do not conform to the homogeneity of variance, the nonparametric test (Kruskal-Wallis test) was used, and the multiple tests were corrected by Bonferroni to determine statistical significance. Values of $p < 0.05$ were considered statistically significant. The sample size per group at each time point in this study was similar to those generally employed in the field [6, 24] and was not pre-determined by a sample size calculation. Potential confounders (e.g., animal/cage location) were not controlled.

Results

Physico-chemical characteristics

The cross-sectional structure of the membranes was observed using FE-SEM [Fig. 1A-a]. The results showed all membranes had a bilayer structure with smooth surface on the top and relative rough surface on the bottom. The cross-sectional analysis of the PD membrane revealed a more pronounced bilayer structure compared to the BP and BD membranes [Fig. 1A-a]. The rough surfaces of all three groups displayed gross undulations and a fibrous texture [Fig. 1A-c], while the smooth surfaces exhibited a less exaggerated topography [Fig. 1A-b]. It is

noteworthy that the smooth surfaces of the BP and PD membranes manifested a higher density in comparison to that of the BD membrane, indicating a potentially superior barrier function for the BP and PD membranes [Fig. 1A-b]. Optical images and roughness measurements supported the FE-SEM results, showing a lower Ra value for the smooth surfaces of the BP and PD membranes in comparison to the BD membrane [Fig. 1B, Table 1]. On the other hand, the PD membrane had the highest Ra value on the rough surface, suggesting a more spatially loose filamentous structure [Table 1].

Table 1: The roughness evaluation of three membranes by white light interferometry

Group	Roughness (Ra, μm)	
	Smooth surface	Rough surface
PD	9.1 ± 0.3	19.8 ± 4.2
BP	7.5 ± 1.2	7.5 ± 0.9
BD	9.0 ± 1.3	10.4 ± 1.1

Abbreviations: Ra, the arithmetic mean deviation of the profile. Data were expressed as mean ± standard deviations (n=3).

In Figure 1C, the BD membrane demonstrated a more rapid degradation rate in vitro. After 5 minutes of enzymatic digestion, the BD membrane became invisible, and was completely degraded after 15 minutes, a timeline comparable to that of the PD membrane. In comparison, the BP membrane underwent a slower degradation process, showing ongoing degradation even beyond the final time point [Fig. 1C].

FTIR was used to assess the integrity of the collagen triple helical structure in all samples. The peaks corresponding to amide A (3300 cm^{-1}), I (1630 cm^{-1}), II (1545 cm^{-1}), and III (1235 cm^{-1}) remain unchanged, indicating that the processing methods for all three membranes did not compromise the collagen structure [Fig. 1D]. Additionally, the typical amide B band of collagen of the BP and BD membranes was observed at 2919 and 2939 cm^{-1}, respectively. Notably, the FTIR spectra obtained from the BD membrane showed a distinct peak at a wavelength of 2116 cm^{-1}.

Contact angle measurements in Figure 1E-F showed that the BP membrane exhibited the highest contact angle and required the longest duration to absorb a water droplet compared to the PD membrane, indicating diminished hydrophilicity. Despite this, the PD and BP membranes had significantly higher water absorption rates than the BD membrane, implying enhanced water retention capabilities for the PD and BP membranes.

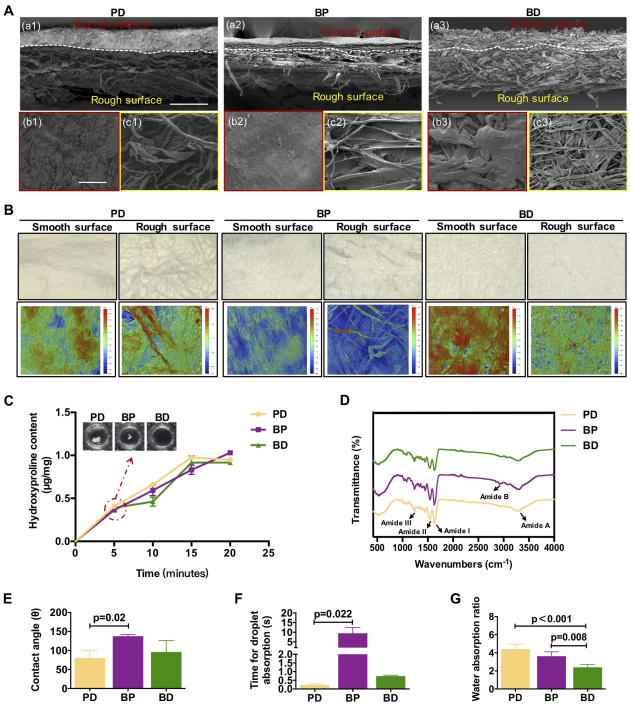

Figure 1: Characterization of three membranes. (A) The microstructures of three membranes on the (a) cross-section, (b) smooth surfaces and (c) rough surfaces using FE-SEM. (B, up) Morphological structures of the smooth and rough surfaces of three membranes observed by optical microscopy. (B, down) The topography of the smooth and rough surfaces of three membranes examined by white light interferometry. (C) Evaluation of the degradation performance of three membranes through hydroxyproline assays (n=3). (D) Elemental composition (including C, O, N, etc.) and organic functional groups on the material surfaces detected by FTIR. (E) Contact angle (n=3), (F) droplet absorption time measurements (n=3), and (G) water absorption ratio (n=4) of three membranes.

Assessment of tissue responses and degradation towards collagen membranes

We next evaluated the three membranes on the tissue responses and degradation in the cranial bone defect of SD rats. Macroscopic photographs (top-right inset) and histological HE-stained tissue sections at low and high magnifications were taken at 1 and 2 weeks post-implantation, as shown in Figure 2B and 2C. The low magnification images in the top row of Figure 2B showed that all implanted membranes (labeled as "M") remained intact at 1 week post-implantation. The distinct porous structure was visible in all three collagen membranes, with only the PD membrane displaying an evident Janus structure (dense layer facing up and porous layer facing down). The high magnification images in the second row of Figure 2B illustrated that fibroblast cells of the connective tissue were observed to grow along the smooth surfaces (labeled as "SS") of PD and BP membranes, without penetrating the interior. In contrast, the BD membrane showed infiltration of fibroblasts, along with a significant presence of monocytes and MNGCs within its interior. The images of the third row in the Figure 2B displayed cellular ingrowth into rough surfaces (labeled as "RS")

of the three membranes, indicating that the porous structure provided the necessary three- dimensional space for the inward growth of cells or tissues. However, a significant presence of MNGCs was observed at the interface of the BD membrane, suggesting a strong foreign body reaction.

Macroscopic photographs of Figure 2C (top-right inset in the top row) revealed that after 2 weeks, the three membranes remained relatively intact, and a complete layer of connective tissue had formed on the smooth surfaces compared to the first week. Consistently, the images in the second row illustrated that the smooth surfaces of the three membranes gradually developed a thin reactive tissue wall with multilayer fibroblasts. Interestingly, the PD and BD membranes showed a higher infiltration of immune cells and fibroblasts within the membrane compared to the BP membrane, indicating that the BP membrane may offer a superior physical barrier against fibrous tissue penetration. The images of the rough surfaces in the third row revealed that, in comparison to the first week, the exudate at the interface between the PD and BP membranes gradually subsided to form cell-active granulation tissue. In this tissue, the PD membrane formed newly formed bone matrix (labeled as “BM”), while BD still contained a significant amount of exudate and lymphocytes.

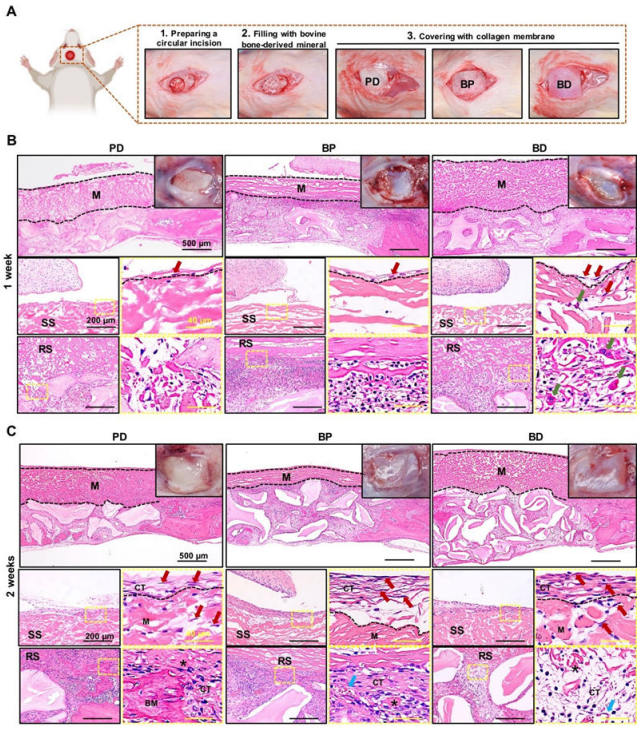

Figure 2: (A) Schematic illustration of the modeling process for the rat cranial bone defect model. (B-C) Evaluation of early local inflammatory responses to three membranes at 1 and 2 weeks post-implantation. Optical images, H&E staining images with different magnifications for the three membranes [Note: black dotted line indicated the area of residual implanted materials, labeled as "M"; SS, smooth surface; RS, rough surface; BM, newly formed bone matrix within the membrane; CT, connective tissue; black asterisk (*) marked membrane fragment; red arrows marked fibroblast; green arrows marked multinucleated giant cells; blue arrows marked blood vessel].

Figure 3A presented macroscopic photographs and histological HE sections taken at 4 weeks post-implantation. Macroscopic photographs (top-right inset) showed that after 4 weeks, the relatively intact membrane material was still visible in the BP and BD membranes, whereas only partial material could be observed in the PD membrane. Additionally, vascular formation was seen on the connective tissue of the smooth surface in the PD and BP membranes. High-magnification HE images revealed that the membranes in the three membranes underwent varying degrees of degradation at 4 weeks post-implantation. The second row of Figure 3A depicted the smooth surfaces of the PD and BP membranes exhibiting partial degradation while retaining their main structure to uphold their barrier function. Corresponding with the macroscopic photographs, HE images revealed numerous vessels on the smooth surfaces of the PD and BP membranes. In contrast, the BD membranes exhibited a distinct membrane interface with increased fibroblast invasion in the membrane's interior, although immune cell infiltration was reduced compared to 2 weeks post-implantation and no significant vascularization was observed. The rough surfaces of the three membranes exhibited notable degradation, as illustrated in Figure 3A, the third row. Both the PD and BP membranes displayed newly formed bone matrix within the membrane. In contrast, the BD membrane did not show newly formed bone matrix within the membrane, but instead exhibited an increase in vessels at the interface.

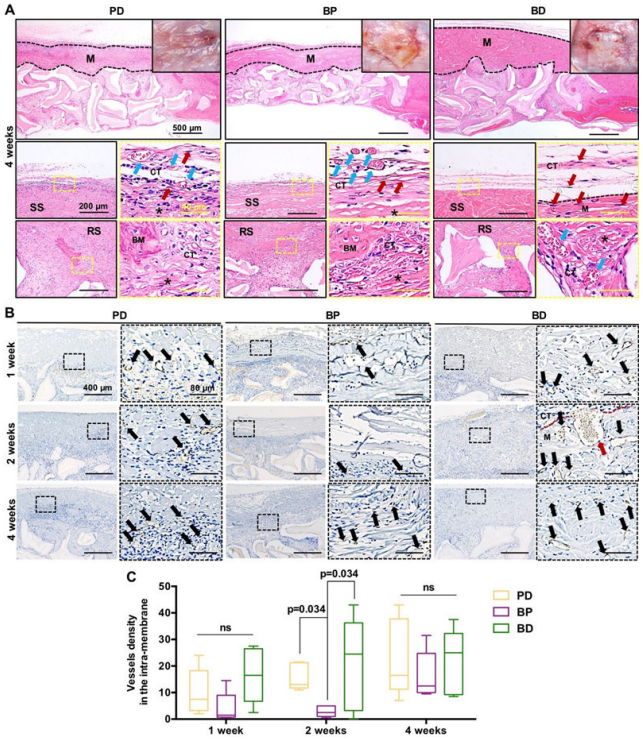

Figure 3: (A) Tissue responses and degradation to three membranes at 4 weeks post implantation. Optical images, H&E staining images with different magnifications for the three membranes [Note: black dotted line indicated the area of residual implanted materials, labeled as “M”; SS, smooth surface; RS, rough surface; BM, newly formed bone matrix within the membrane; CT, connective tissue; black asterisk (*) marked membrane fragment; red arrows marked fibroblast; blue

arrows marked blood vessel]. (B) The images and (C) the number of stained vessels per 100x, i.e., the vessel density (vessels/per 100x) in the areas of intra-membrane at 1, 2 and 4 weeks post implantation. [Note: black arrows marked blood vessel]. (CD31 immunostaining, n=5).

After 8 weeks of implantation, significant degradation of the three membranes was observed, leading to an incomplete membrane structure as depicted in Figure 4A, the top row. Material remnants were still visible in the BP membrane up to 12 weeks, whereas the PD and BD membranes were no longer visible at week 12 [Fig. 5A, topleft inset]. Following the 8-week mark [Fig. 4A, the second row], a multi-layered loose connective tissue resembling normal periosteal morphology [Fig. 5E] began to form gradually on the smooth surfaces of the PD and BP groups. In contrast, dense fibrous connective tissue persisted at the BD group interface until the 12-week mark [Fig. 4A, the second row for 8 weeks and Fig. 5A, the second row for 12 weeks]. After 12 weeks, significant membrane degradation was observed on the rough surface of the three membranes, and the formation of larger blocks of newly formed bone matrix within the membranes was shown in the PD and BP membranes when compared to the BD membrane [Fig. 5A]. By 16 weeks, the three membranes had achieved substantial integration [Fig. 5F]. Notably, no discernible inflammatory fibrous tissue encapsulation was observed for any of the three membranes throughout the observation period, indicating histocompatibility.

The initial thickness of the three membranes in dry condition was measured using FE-SEM [Fig. 1A]. The BD and PD membranes exhibited similar initial thicknesses, ranging from approximately 414-448 μm, while the BP membrane was the thinnest at around 213 μm [Fig. 4E]. Following implantation in vivo for the first 2 weeks, due to the infiltration of blood, exudate and cells, all three membranes showed expansive structures, and subsequent decrease, with the turning point at the second week for the PD and BD membranes and the fourth week for the BP membrane. The thickness gradually decreases due to the recession of inflammatory tissue and the degradation of the absorbable membrane over the next 14 weeks. In contrast to the in vitro results, the PD membrane degraded most rapidly in vivo, achieving almost complete degradation by 16 weeks. In comparison, the other two membranes showed remnants of degradation, suggesting incomplete dissolution, particularly for the BD membrane [Fig. 4E].

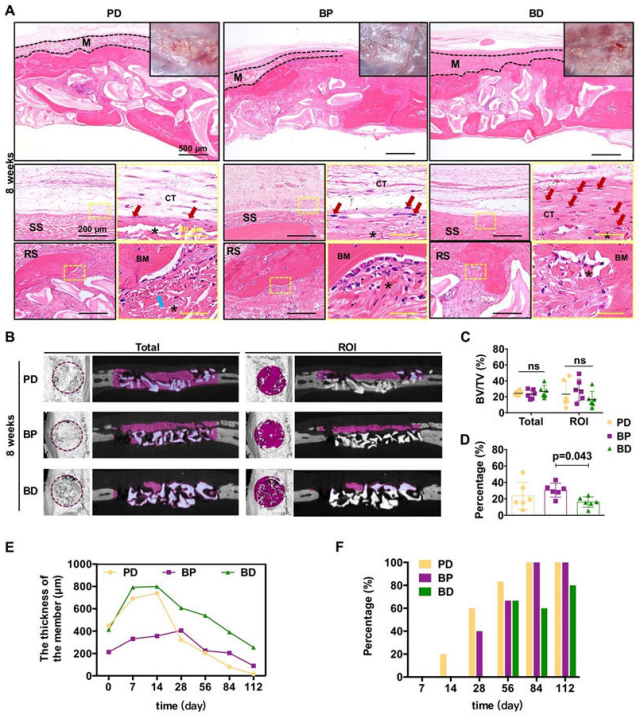

Figure 4: (A) Tissue responses and degradation to three membranes at 8 weeks post implantation. Optical images, H&E staining images with different magnifications for the three membranes [Note: black dotted line indicated the area of residual implanted materials, labeled as "M"; SS, smooth surface; RS, rough surface; BM, newly formed bone matrix within the membrane; CT, connective tissue; black asterisk (*) marked membrane fragment; red arrows marked fibroblast; blue arrows marked blood vessel]. (B) Observation of bone formation in the total defect area (Total, diameter of 6 mm, height of 2 mm) and adjacent to the membrane (ROI, diameter of 6 mm, height of 0.5 mm) using Micro-CT at 8 weeks. (C) Bone volume/total volume (BV/TV) values of Total and ROI at 8 weeks (n=6). (D) Contribution ratio of ROI bone formation to the total bone formation in the defect area at 8 weeks (n=6). Comparison of (E) membrane thickness changes and (F) the proportion of bone formation within the membrane after implantation for the three membranes.

Vascularization of collagen membranes

The vascularization of the three membranes was compared at 1, 2, and 4 weeks post-implantation. In Figure 3B, vessels ingrowth into the PD and BD membranes was primarily concentrated in the rough layer at 1 week post-implantation, with faster collagen membrane decomposition correlating with higher vessel ingrowth levels. Conversely, only a few vessels were present in the BP membrane at the same time point. By 2 weeks post-implantation, vessels in the PD and BD membranes continued to be predominantly located in the rough layer before gradually penetrating towards the middle of the membrane, accompanied by an increase in vessel diameter compared to the first week, particularly in the BD membrane. However, angiogenesis in the BP membrane remained below that of the other two membranes. At 4 weeks post- implantation, as the PD membrane integrated further, more vessels were concentrated at

the edge. The number of vessels in the BP membrane showed gradual increase compared to previous time points.

In Figure 3C, the quantitative results of membrane vascularization indicated that, over the observation period, the vessel density of the BD membrane was superior than that of the other two membranes. Conversely, the vessel density in the BP membrane was the lowest, particularly at 2 weeks post-implantation, where it was significantly lower than that of both the BD and PD membranes.

Osteogenic effects of collagen membranes

Membrane ossification was distinctly observed in both PD and BP membranes by 4 weeks, whereas in the BD membranes, this phenomenon occurred later and was not detected until 8 weeks [Fig. 4F]. Prior to 8 weeks, the PD membrane exhibited a higher percentage of ossification compared to the BP membrane, with both membranes achieving similar levels after 12 weeks. In contrast, the ossification percentage of the BD membrane consistently remained lower than that of the other two membranes [Fig. 4F].

No significant differences in osteogenic effect, as measured by bone volume fraction (BV/TV), was observed among the three membranes at 8 and 12 weeks in both the total defect area [diameter of 6 mm, height of 2 mm] and the area adjacent to the membrane [diameter of 6 mm, height of 0.5 mm] [8 weeks, Fig. 4B-C; 12 weeks, Fig. 5B-C]. This lack of variation may be attributed to the primary osteogenic effect within the defect area being associated with the bone substitute materials, thus maintaining consistency across all three membranes. Interestingly, when examining the proportion of bone formation adjacent to the membrane to the total bone formation in the defect area, the BP membrane showed the highest proportion of membrane-adjacent bone formation at 8 weeks, surpassing that of the BD membrane [Fig. 4D)]. By 12 weeks, the PD membrane exhibited the highest proportion of adjacent bone formation, notably higher than the BD membrane [Fig. 5D].

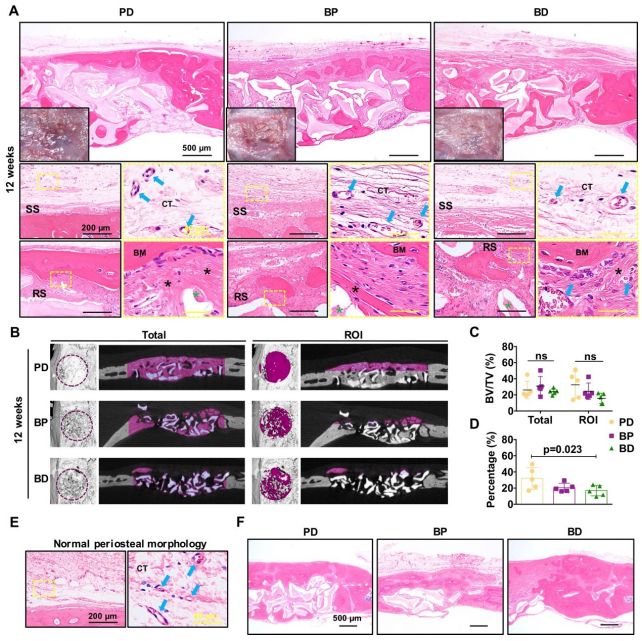

Figure 5: (A) Tissue responses and degradation to three membranes at 12 weeks post implantation. Optical images, H&E staining images with different magnifications for the different membranes [Note: black dotted line indicated the area of residual implanted materials, M; SS, smooth surface; RS, rough surface; BM, newly formed bone matrix within the membrane; CT, connective tissue; black asterisk (*) marked membrane fragment; green asterisk (*) marked calcined bovine bone remnants; blue arrows marked blood vessel]. (B) Observation of bone formation in the total defect area (Total, diameter of 6 mm, height of 2 mm) and adjacent to the membrane (ROI, diameter of 6 mm, height of 0.5 mm) using Micro-CT at 12 weeks. (C) Bone volume/total volume (BV/TV) values of total and ROI at 12 weeks (n=5). (D) Contribution ratio of ROI bone formation to the Total bone formation in the defect area at 12 weeks (n=5). (E) The HE histological images showing normal periosteal morphology. (F) The HE staining images for the different membranes for 16 weeks post implantation.

DISCUSSION

This study compared the properties of collagen membranes sourced from Bovine Pericardium (BP) and Bovine Dermis (BD) with Porcine-Derived dermis membranes (PD). The aim was to investigate how the source of collagen influences tissue reactions. The cranial bone defect model of SD rats was employed to assess the effectiveness of the membranes as barriers, as well as their roles in bone regeneration and degradation processes. Results indicated that compared to the porcine-derived dermis collagen membrane, the bovine-derived pericardium collagen membrane had an optimal degradation behavior as well as a superior barrier function, and showed comparable results in terms of bone regeneration and soft healing.

In this study, all the three membranes had a bilayer structure composed of one smooth surface and one rough surface. Differences were present in the morphology among the three membranes, especially for the smooth surface. The smooth surfaces of the BP and PD membranes manifested a higher density in comparison to that of the BD membrane, suggesting that the BP and PD membranes may have a better barrier function. Interestingly, the FTIR spectra taken from the BP and BD membranes showed amide A, amide B, amide I, amide II, and amide III, the typical bands for collagen type I [25]. However, the BD membrane showed a poorly defined band with impurities (2116 cm-1) [25], which may be the reason for the strong foreign body reaction in vivo. And the FTIR spectra taken from the PD membrane was lacking in the typical amide B band. These results illustrated that although the integrity of the collagen triple helical structure was present in all membranes, the BP membrane had the well-defined and expected type I collagen with higher degree of purity. The membranes described above differ not only with respect to their architecture but also in relation to initial thickness, which may influence their mechanical and space maintaining properties during implantation [20, 26]. The membranes of the BD and PD membranes presented a relatively robust initial thickness at

approximately 414-448 μm, while the membranes of the BP group measured approximately 213 μm, as the thinnest one.

After immediately implanting, the body triggers a series of reactions to the injury, including the blood–material interaction, the formation of a provisional matrix, acute inflammation, development of granulation tissue and foreign body reactions [27]. These events involve the activation and differentiation of various cells, such as polymorphonuclear leukocytes, monocytes/macrophages, MNGCs, lymphocytes and even fibroblasts. By virtue of their early recruitment to the site of healing and their wide secretory profile, monocytes/macrophages have been suggested as a potent moderator of the healing events [28]. From the histological results in this study, the PD and BP groups induced mainly monocytes/macrophages in the early post-implantation period and these cells started to penetrate into the central region of the material from both surfaces. However, the BD membrane induced monocytes/macrophages and together with some MNGCs in the early post-imiplantation period. The presentation of MNGCs might mean a higher or more pro-inflammatory alignment of the material-associated tissue reaction, leading to poor tissue regeneration [29]. Al-Maawi et al. has found that the biomaterial-induced MNGCs showed common characteristics with pathological MNGCs (Langerhans' giant cells) that exist in sarcoidosis and tuberculosis [30]. And it has been revealed that the presence of more phagocyting cells, such as macrophages and MNGCs, might correlate with fast membrane degradation and a higher transmembraneous vascularization [8, 10, 31].

In the context of GBR procedures, especially implanted-bed vascularization via angiogenesis has been recognized as a basic factor for successful bone regeneration [14, 32]. The transmembraneous vascularization mainly refers to the vessel formation within a membrane to bridge especially longer distances, as in the case of thicker barrier membranes [33]. Nevertheless, previous studies have shown that naturally collagen- derived membranes from porcine or bovine dermis do not require transmembranous vascularization for successful bone integration6, [10, 34, 35]. The central portions of these materials can be supplied with nutritive elements by processes such as diffusion, which are present in well-vascularized tissues, such as the oral cavity [10]. In this study, vessels were unable to completely penetrate the membranes and formed a vascular network between the collagen fibers during the observation period [Fig. 3B]. Interestingly, the results in the Figure 3C reflected another issue that an exuberant vascularization may not contribute to its tissue regeneration function. The BD membrane had a high vessel density, but it had a poor tissue integration and osteogenic performance. The increased vascularization of the BD membrane may be related to the formation of MNGCs, which provide the source of angiogenic molecules, such as the Vascular Endothelial Growth Factor (VEGF), not contributing to its tissue regeneration function [36-37]. As described in the previous study [38], the changes in the cellular reaction and vascularization within the BD membrane were related typical indications of a foreign body reaction. Unlike the BD membrane, the BP and PD membranes did not induce a well-vascularized granulation tissue, especially for the BP membrane. It appeared as if the host inflammatory response complex recognized the membrane of the BP membrane as an endogenous collagen and did not treat it as a foreign body. It is known that microvessels can supply tissues with oxygen for distances of between 100 and 200 μm [39]. Due to the relatively thin thickness (<400 μm) of the BP membrane throughout the observation period, mild vascularization might provide nutrients that help to generate an appropriate niche environment for osteoprogenitors and improve bone repair, which is attributable to its tissue source [18, 35, 40].

Recent experimental researches have shown that collagen membranes' degradation can commence 4 to 28 days after implantation [5, 41]. In GBR, a minimum period of 3 to 4 weeks is required to ensure the cells' repopulation and maturation that form the bone matrix. Some scholars also suggest that ideal GBR membranes should maintain its barrier function for 16–24 weeks to meet the requirement of different bone augmentation methods [11]. The histological results in this study revealed that these three membranes could serve as a stable material during the first 2-4 weeks after implantation, and without any signs of membrane fragmentation up to the end of the observation period. The PD membrane underwent a nearly complete biodegradation and integration between week 8 and week 16 after implantation, while the other groups still had remnants at week 16, indicative of a longer degradation period. What's more, the degradation rate of the BP membrane was the most stable among the three membranes in vitro and in vivo, suggesting that it is more in line with the requirement of ideal GBR membrane and has the advantage of lowering the risk of soft tissue dehiscence [42]. This could be attributed to the higher content of type I collagen in the BP membrane, which is known to be more resistant to degradation compared to type III collagen [35]. Interestingly, these three membranes in this study disintegrated into smaller subunits that were further surrounded by a cell-rich tissue. This mode of degradation uses the material as a porous guide for the surrounding connective tissue, and persisted within the implantation bed with integration.

Reaching the balance between the material degradation and the tissue healing process is a serious challenge for absorbable membrane. The compatibility of the barrier membrane needs to allow osteogenic cells to grow from the edge of the existing bone to form new bone tissue structure and achieve bone regeneration1. According to the histological results in this study, at the early stage (before week 4), bone formed predominantly in the bottom and peripheral regions of the defect, whereas the top regions (within and underneath the membrane) gained a significant amount of bone in the late phase (after week 8). These results may be attributed to the special degradation mode of these three membranes, especially on the rough surfaces, gradually generating a porous guide for the surrounding connective tissue over time, and promoting the material-induced infiltration of immune cells (e.g., monocytes/macrophages) and histiocytes (osteoblasts or mesenchymal stem cells) [8, 43]. And the environment created by the membranes could be conducive to the formation and reconstruction of the molecular mechanism of coupled bone in the submembrane defect [44]. Membrane ossification was observed in both PD and BP membranes by 4 weeks, whereas the manifestation of this phenomenon in the BD membrane occurred later (at 8 weeks).

It was speculated that the microenvironment created directly under the membranes of the BP and PD membranes provided osteoinductive signals that rapidly promoted newly formed bone matrix in the top regions [43]. And this preferential effect of the membrane- induced microenvironment on bone regeneration in the top regions extended to the late stage for the BP and PD membranes. Although the primary osteogenic effect within the defect area is correlated with the bone substitute materials, we found that the BP and PD membranes contributed a higher proportion of membrane-adjacent bone formation compared to the BD membrane at 8 and 12 weeks.

Moreover, GBR surgery requires good soft tissue sealing and long-term wound stability to protect the regenerative process [45]. A distinguishing factor of absorbable membranes compared to non-absorbable PTFE, is having not only a barrier function but also soft tissue integration that can potentially enhance the wound healing and bone regeneration [44]. In this study, we observed that the smooth surfaces on the PD and BP membranes formed a single layer of fibroblast cells at 1 week, then developing to a thin reactive tissue wall with multilayer fibroblasts at 2 weeks and performing multi-layered loose connective tissue similar to the normal periosteal morphology until 8 weeks. Therein, for the BP membrane, fibroblast cells of connective tissue only grew along the membrane's smooth surfaces without penetrating the membrane's interior, which was related to its lower roughness on the smooth surfaces, as a denser structure to prevent fibrous tissue invasion. In contrast, an infiltration of fibroblasts as well as a large number of monocytes and MNGCs was seen with the BD membrane's interior at the early stage, and multi-layered loose connective tissue similar to the normal periosteal morphology was just performed until 12 weeks. These results suggest that the membranes of the BP membrane are superior to those of the PD and BD membranes as a barrier to prevent fibrous tissue invasion.

However, this study has potential limitations. One major limitation was the unclear mechanism by which collagen fibers from bovine-sourced pericardium collagen membrane promoted osteogenic differentiation. Further analysis at the cellular and molecular levels is necessary. Another limitation was the small number of animals, which is driven by a desire to minimize the burden of experimental animals. Our following research will use more animals and large mammals to obtain more reliable and predictable data.

CONCLUSION

Three xenogeneic collagen membranes from different animal species and tissues were analyzed in this study to determine the most suitable source of natural collagen for GBR. The BP membranes exhibited optimal degradation behavior, superior barrier function, and bone regeneration potential, making it a promising candidate for ideal GBR membranes. The anisotropic Janus microstructure of BP membrane effectively fulfilled both functions, with its smooth surface acting as a barrier against fibrous tissue invasion and promoting soft tissue healing, while the rough surface supported bone regeneration. The findings shed light on the diverse responses of hosts to collagen membranes from different sources, allowing for tailored composites that can address specific clinical needs in both hard and soft tissue regeneration scenarios.

DECLARATION OF COMPETING INTEREST

The authors have no conflicts of interest relevant to this article.

ACKNOWLEDGEMENTS

This work was supported by the National Natural Science Foundation of China (No. 82271026) and Start-up Fund of Stomatology Hospital, School of Stomatology, Zhejiang University School of Medicine (2023PDF017).

REFERENCES

1. Yang Z, Wu C, Shi H, Luo X, Sun H, Wang Q, Zhang D. Advances in barrier membranes for guided bone regeneration techniques. Front Bioeng Biotechnol. 2022; 10:921576.
2. Ren Y, Fan L, Alkildani S, Liu L, Emmert S, Najman S, Rimashevskiy D, Schnettler R, Jung O, Xiong X, Barbeck M. Barrier membranes for guided bone regeneration (GBR): a focus on recent advances in collagen membranes, J Mol Sci. 2022;23(23):14987.
3. Wang HL, Carroll WJ. Guided bone regeneration using bone grafts and collagen membranes. Quintessence international. 2001;32(7).
4. Hürzeler M. B, Kohal R. J, Naghshbandl J, Mota L F, Conradt J, Hutmacher D, Caffesse R. G. Evaluation of a new bioresorbable barrier to facilitate guided bone regeneration around exposed implant threads: An experimental study in the monkey. Int J Oral Maxillofac Surg. 1998;27(4):315-320.
5. Owens KW, Yukna RA. Collagen membrane resorption in dogs: a comparative study. Implant Dent. 2001;10(1):49-58.
6. Kapogianni E, Alkildani S, Radenkovic M, Xiong X, Krastev R, Stöwe I, Bielenstein J, Jung O, Najman S, Barbeck M, Rothamel D. The early fragmentation of a bovine dermis-derived collagen barrier membrane contributes to transmembraneous vascularization—A possible paradigm shift for guided bone regeneration. Membr. 2021;11(3):185.
7. Ghaemmaghami A, Martin, Harmsen M, Kargozar S, Ghanaati S, Al-Maawi S, Vorakulpipat C, Orlowska A, Zrnc T A, Sader R A. In vivo implantation of a bovine-derived collagen membrane leads to changes in the physiological cellular pattern of wound healing by the induction of multinucleated giant cells: an adverse reaction?. Front Bioeng Biotechnol. 2018;6:104.
8. Barbeck M, Lorenz J, Holthaus M G, Raetscho N, Ghanaati S. Porcine Dermis and Pericardium-Based, Non–Cross-Linked Materials Induce Multinucleated Giant Cells After Their In Vivo Implantation: A Physiological Reaction?. J Oral Implantol. 2015;41(6):e267-281.
9. Rothamel D, Schwarz F, Sager M, Herten M, Becker J. Biodegradation of differently cross-linked collagen membranes: an experimental study in the rat. Clin Oral Implants Res. 2005;16(3): 369-378.
10. Barbeck M, Lorenz J, Kubesch A, Booms P, Boehm N, Choukroun J, Sader R, Kirkpatrick C. J, Ghanaati S. Porcine dermis-derived collagen membranes induce implantation bed vascularization via multinucleated giant cells: a physiological reaction?. J Oral Implantol. 2015;41(6):e238-251.
11. Hoornaert A, D'Arros C, Heymann M. F, Layrolle P. Biocompatibility, resorption and biofunctionality of a new synthetic biodegradable membrane for guided bone regeneration. Biomed. Mater. 2016;11(4):045012.
12. Rothamel D, Schwarz F, Fienitz T, Smeets R, Zoller J. Biocompatibility and biodegradation of a native porcine pericardium

membrane: results of in vitro and in vivo examinations. Int. J. Oral Maxillofac. Implants. 2012;27(1).

13. Gupta S, Gupta R. Guided bone regeneration with pericardium membranes. IOSR J. Dent. Med. Sci. 2014;13(11):61-65.
14. Schwarz F, Rothamel D, Herten M, Sager M, Jurgen Becker. Angiogenesis pattern of native and cross-linked collagen membranes: an immunohistochemical study in the rat. Clin. Oral Implants Res. 2006;17(4):403-409.
15. Hirata H H, Munhoz M A S, Plepis A M. G, Martins V C A, Santos G R, Galdeano E A, Cunha M R.. Feasibility study of collagen membranes derived from bovine pericardium and intestinal serosa for the repair of cranial defects in ovariectomised rats. Injury. 2015;46(7):1215-1222.
16. Yamanaka JS, Oliveira AC, Bastos AR, Fernandes EM, Reis RL, Correlo VM, Shimano AC. Collagen membrane from bovine pericardium for treatment of long bone defect. J Biomed Mater Res B Appl Biomater. 2023;111(2):261-270.
17. Lynn AK, Yannas IV, Bonfield W. Antigenicity and immunogenicity of collagen. J Biomed Mater Res B Appl Biomater. 2004;71(2): 343-354.
18. Moura CC, Soares PB, Carneiro KF, Souza MA, Magalhaes D. Cytotoxicity of bovine and porcine collagen membranes in mononuclear cells. Braz Dent J. 2012;23:39-44.
19. Parenteau-Bareil R, Gauvin R, Cliche S, Gariepy C, Germain L, Berthod F. Comparative study of bovine, porcine and avian collagens for the production of a tissue engineered dermis. Acta Biomater. 2011;7(10):3757-3765.
20. Elgali I, Omar O, Dahlin C, Thomsen P. Guided bone regeneration: materials and biological mechanisms revisited. Eur J Oral Sci. 2017;125(5):315-337.
21. Gu J T, Jiao K, Li J, Yan J F, Wang KY, Wang F, Liu Y, Tay FR, Chen JH, Niu LN. Polyphosphate-crosslinked collagen scaffolds for hemostasis and alveolar bone regeneration after tooth extraction. Bioact Mater. 2022;15:68-81.
22. Lindner C, Prhl A, Abels M, Lffler T, Barbeck M. Specialized histological and histomorphometrical analytical methods for biocompatibility testing of biomaterials for maxillofacial surgery in (pre-) clinical studies. In Vivo. 2020;34(6):3137-3152.
23. Alkildani S, Ren Y, Liu L, Rimashevskiy D, Schnettler R, Radenkovic M, Najman S, Stojanovic S, Jung O, Barbeck M. Analyses of the cellular interactions between the ossification of collagen-based barrier membranes and the underlying bone defects. Int J Mol Sci. 2023;24(7):6833.
24. Radenkovic M, Alkildani S, Stoewe I, Bielenstein J, Sundag B, Bellmann O, Jung O, Najman S, Stojanovic S, Barbeck M. Comparative in vivo analysis of the integration behavior and immune response of collagen-based dental barrier membranes for guided bone regeneration (GBR). Membr. 2021;11(9):712.
25. Riaza T, Zeeshana R, Zarifa F, Ilyasa K, Muhammada N, Safia SZ, Rahima A, Rizvib SAA, Rehmanc I U. FTIR analysis of natural and synthetic collagen. Appl Spectrosc Rev. 2018;53(9):703-746.
26. Aprile P, Letourneur D, Simon-Yarza T. Membranes for guided bone regeneration: a road from bench to bedside. Adv Healthc Mater. 2020;9(19):2000707.
27. Anderson JM, Rodriguez A, Chang DT. Foreign body reaction to biomaterials. Semin. Immunol. 2008; 20 (2): 86-100.
28. Thomsen P, Gretzer C. Macrophage interactions with modified material surfaces. Curr Opin Solid State Mater Sci. 2001;5(2-3): 163-176.
29. Miron RJ, Bosshardt DD. Multinucleated giant cells: good guys or bad guys?. Tissue Eng Part B Rev. 2018;24(1):53-65.
30. Al-Maawi S, Orlowska A, Sader R, Kirkpatrick CJ, Ghanaati S. In vivo cellular reactions to different biomaterials—Physiological and pathological aspects and their consequences. Semin Immunol. 2017; 29:49-61.
31. Tanneberger AM, Al-Maawi S, Herrera-Vizcaino C, Orlowska A, Ghanaati S. Multinucleated giant cells within the in vivo implantation bed of a collagen-based biomaterial determine its degradation pattern. Clin Oral Investig. 2021;25:859-873.
32. Kaarevi EP, Rider P, Alkildani S, Retnasingh S, Pejaki M, Schnettler R, Gosau M, Smeets R, Jung O, Barbeck M. An introduction to bone tissue engineering. Int J Artif Organs. 2020;43(2):69-86.
33. Delgado LM, Bayon Y, Pandit A, Zeugolis DI. To cross-link or not to cross-link? Cross-linking associated foreign body response of collagen-based devices. Tissue Eng. Part B Rev. 2015;21(3):298-313.
34. Ghanaati S, Schlee M, Webber M J, Willershausen I, Kirkpatrick C J. Evaluation of the tissue reaction to a new bilayered collagen matrix in vivo and its translation to the clinic. Biomed Mater. 2011;6(1):015010.
35. Ghanaati S. Non-cross-linked porcine-based collagen I–III membranes do not require high vascularization rates for their integration within the implantation bed: A paradigm shift. Acta Biomater. 2012;8(8): 3061-3072.
36. Barbeck M, Booms P, Unger R, Hoffmann V, Sader R, Kirkpatrick CJ, Ghanaati S. Multinucleated giant cells in the implant bed of bone substitutes are foreign body giant cells—New insights into the material-mediated healing process. J Biomed. Mater Res A. 2017;105(4): 1105-1111.
37. Barbeck M, Udeabor SE, Lorenz J, Kubesch A, Choukroun J, Sader RA, Kirkpatrick, CJ, Ghanaati S. Induction of multinucleated giant cells in response to small sized bovine bone substitute (Bio-Oss™) results in an enhanced early implantation bed vascularization. Ann Maxillofac Surg. 2014;4(2):150-157.
38. Ghaemmaghami A, Martin, Harmsen M, Kargozar S, Ghanaati S, Al-Maawi S, Vorakulpipat C, Orlowska A, Zrnc TA, Sader RA. In vivo implantation of a bovine-derived collagen membrane leads to changes in the physiological cellular pattern of wound healing by the induction of multinucleated giant cells: an adverse reaction?. Front Bioeng Biotechnol.2018;6:104.
39. Dew L, MacNeil S, Chong CK. Vascularization strategies for tissue engineers. Regen Med. 2015;10(2):211-224.
40. Kusumbe AP, Adams RH. Osteoclast progenitors promote bone vascularization and osteogenesis. Nat Med. 2014;20(11):1238-1240.
41. Zhao S, Pinholt EM, Madsen JE, Donath K. Histological evaluation of different biodegradable and non-biodegradable membranes implanted subcutaneously in rats. J Craniomaxillofac Surg. 2000;28(2):116-122.
42. Sbricoli L, Guazzo R, Annunziata M, Gobbato L, Bressan E, Nastri L. Selection of collagen membranes for bone regeneration: A literature review. Mater. 2020;13(3):786.
43. Turri A, Elgali I, Vazirisani F, Johansson A, Emanuelsson L, Dahlin C, Thomsen P, Omar O. Guided bone regeneration is promoted by the molecular events in the membrane compartment. Biomaterials. 2016;84:167-183.
44. Omar O, Elgali I, Dahlin C, Thomsen P. Barrier membranes: More than the barrier effect?. J Clin Periodontol. 2019;46:103-123.
45. Wang HL, Boyapati L. "PASS" principles for predictable bone regeneration. Implant Dent. 2006;15(1):8-17.